

Mean-field Wigner function of Bose–Einstein condensates in the Thomas–Fermi limit

J Teske, M R Besbes, B Okhrimenko and R Walser

Institut für Angewandte Physik, Technische Universität Darmstadt, Hochschulstrasse 4A, 64289 Darmstadt, Germany

E-mail: jan.teske@physik.tu-darmstadt.de

Received 2 July 2018, revised 5 September 2018

Accepted for publication 28 September 2018

Published 26 October 2018



Abstract

We study the mean-field phase-space distribution of the ground state of an anisotropic, harmonically trapped Bose–Einstein condensate at zero temperature. First, we derive the Fourier transform of the ground-state wave function in the Thomas–Fermi limit in d dimensions. Second, we obtain analytical approximations for the Thomas–Fermi Wigner function in one and three dimensions with a factorization ansatz of the coherence function. These approximate expressions are compared with exact numerical simulations of the Gross–Pitaevskii equation.

Keywords: phase-space distribution, Bose–Einstein condensates, matter waves, Thomas–Fermi limit, Wigner function

(Some figures may appear in colour only in the online journal)

1. Introduction

The wave nature of massive particles is one of the many counter-intuitive phenomena in quantum mechanics that we have to accept. In 1924, it was foreseen by L De Broglie [1] and two years later, observed in electron diffraction by C Davisson and L Germer [2]. A century has passed and we are still puzzled by the fact. However, we have learned sundry clever means to utilize the interference of atomic matter waves [3, 4] for technical purposes, for example, as high precision acceleration sensors probing gravity on earth [5–9], and in space [10, 11].

New states of matter were predicted by A Einstein [12, 13] in 1924 and gaseous atomic Bose–Einstein condensates were created in 1995 by E Cornell, C Wiemann and W Ketterle [14–16]. Atomic Bose–Einstein condensates are now routinely used as coherent sources for macroscopic matter waves and are manipulated by mirrors, beam splitters, atomic waveguides and lenses [17–21].

In 1932 E Wigner invented a quasi-distribution function to represent thermal-, as well as quantum-fields in the corresponding classical phase space [22]. All classical-, thermal- or quantum-field theories can be described by the symmetric ordered Wigner phase-space distribution [23–26]. Recently, interacting atomic quantum gases are simulated successfully using a truncated Wigner approach to study

finite-temperature ensembles with stochastic classical fields [27–29], or the quantum Boltzmann equation with interactions [30, 31].

Here, we focus at temperatures well below the Bose–Einstein phase-transition temperature, where one can use the Gross–Pitaevskii mean-field equation [32, 33] to describe the coherent mode of the condensate. In the Thomas–Fermi limit [34, 35], when mean-field energies are much larger than the vacuum energy, one can obtain many relevant physical observables like position width, momentum spread, healing length or excitation frequencies in closed form [36, 37].

A closed-form expression of the Wigner function for trapped Bose–Einstein condensate provides a complementary description of matter-wave experiments in phase space. In particular, the scaling laws [38, 39] in the Thomas–Fermi limit provide the correct time-dependence in quadratic external potentials. Therefore, a classical phase-space propagation of matter waves [40–42] benefits from a simple lookup function that exhibits the correct physical properties.

1.1. Dedication

We dedicate this paper to Wolfgang Schleich on the occasion of his 60th birthday. He is an avid promoter of the view on quantum physics from phase space. Complex analysis of interference phenomena become untangled by a simple phase-space

drawing and physical interpretation is feasible. His restless and creative pursuit of nature to reveal its secrets is only surpassed by his splendid humor supported by a treasure chest full of anecdotes. It is a great pleasure to learn from him.

1.2. Outline

Our paper is organized as follows: in section 2, we briefly recall the basics of the Gross–Pitaevskii mean-field theory. In section 2.1, we focus on the Thomas–Fermi limit for repulsive interactions and obtain the Fourier amplitude of the field in a harmonic trap in d dimensions. In section 3, we obtain analytical approximations for the Thomas–Fermi Wigner function within the factorization ansatz of the coherence function and compare these with exact numerical simulations. A conclusion and outlook is given in section 4.

2. Classical field approximation for bosons

The physics of cold dilute atomic gases is determined by the interplay of single-particle motion in an external potential $v(\mathbf{r})$ and the internal energy $gn(\mathbf{r})$ arising from the van der Waals interaction [43]. In the s -wave limit, the latter can be described by a contact interaction of strength $g = 4\pi\hbar^2 a_s/m$, with the atomic mass m and the scattering length a_s .

Assuming a three-dimensional harmonic trap with an average frequency $\bar{\omega}$ sets the Bose–Einstein phase transition temperature at $T_{\text{BEC}} = \hbar\bar{\omega}N^{1/3}/k_B$ for a gas of N atoms [44]. For temperatures $T \ll T_{\text{BEC}}$, essential physics can be described by the classical Gross–Pitaevskii field approximation $\psi(\mathbf{r}, t)$ [45–47]

$$i\hbar\partial_t\psi(\mathbf{r}, t) = \left[-\frac{\hbar^2}{2m}\nabla^2 + v(\mathbf{r}) + gn(\mathbf{r}, t) \right] \psi(\mathbf{r}, t), \quad (1)$$

$$N = \int d^d r n(\mathbf{r}, t). \quad (2)$$

Here, the atomic density $n(\mathbf{r}, t) \equiv |\psi(\mathbf{r}, t)|^2$ is normalized to the particle number N .

Classical fields are useful physical approximations in dimensions $d \geq 3$, when fundamental quantum fluctuation are less important [48, 49]. However, in trapped gases these approximations can also be extended to lower dimensions $d = 1, 2$, when the motion in other spatial directions is ‘frozen-out’, thus obtaining an effective lower dimensional mean-field theory [50]. Therefore, we will consider the non-linear Schrödinger equation (1) in d dimensions at fixed coupling constant g and variable particle number N .

2.1. Thomas–Fermi approximation

In the stationary case the time-dependent field is governed by $\psi(\mathbf{r}, t) = e^{-i\mu t/\hbar}\psi(\mathbf{r})$, where $\mu(N)$ is the chemical potential of the condensate. Thus, the Gross–Pitaevskii equation for stationary field $\psi(\mathbf{r})$ reads

$$\left[-\frac{\hbar^2}{2m}\nabla^2 + v(\mathbf{r}) + gn(\mathbf{r}) - \mu \right] \psi(\mathbf{r}) = 0. \quad (3)$$

In the limit of large repulsive interactions, one can neglect the quantum pressure that arises from the localization energy of the classical field and obtains the Thomas–Fermi approximation

$$[v(\mathbf{r}) + gn_{\text{TF}}(\mathbf{r}) - \mu]\psi_{\text{TF}}(\mathbf{r}) = 0. \quad (4)$$

This equation admits the algebraic solution

$$n_{\text{TF}}(\mathbf{r}) = \begin{cases} \frac{\mu - v(\mathbf{r})}{g} > 0, & \forall \mathbf{r} \in V_{\text{TF}}, \\ 0, & \text{else,} \end{cases} \quad (5)$$

for the density and the corresponding wave function $\psi_{\text{TF}} = \sqrt{n_{\text{TF}}}$. The classical field has a finite support within the Thomas–Fermi volume V_{TF} , which is bounded by the oriented surface $S_{\text{TF}} = \{\mathbf{r} \in \mathbb{R}^d \mid \mu(N) = v(\mathbf{r})\}$. For many purposes, the Thomas–Fermi approximation is very convenient. However, caution is required due to the discontinuous slope, which leads to unphysical divergences [51].

2.2. Thomas–Fermi approximation for anisotropic harmonic oscillators in d dimensions

Atoms can be trapped with optical dipole potentials [52], or by static magnetic fields created by atomic chips [53–57]. Expanding the potential around a minimum \mathbf{r}_0 , conveniently shifting the origin to this location, yields a good local approximation

$$v(\mathbf{r}) = v_0 + \frac{1}{2}\mathbf{r}^T H \mathbf{r} + \mathcal{O}(r^3). \quad (6)$$

Finite anharmonicities do exist and have a detrimental impact on high precision interferometry [11]. However, in many experimental situations, a d -dimensional anisotropic harmonic oscillator potential is a good approximation to start with. For each atomic species with mass m , the positive Hessian matrix H defines a harmonic frequency matrix $\Omega^2 = H/m \in \mathbb{R}^{d \times d}$. In general, the principle axes of the potential are not aligned with the coordinate system of the atom chip. The two coordinates systems are connected by a rotation matrix R defined by

$$\Omega^2 R = R \omega^2. \quad (7)$$

The trap frequencies $\omega_i > 0$ are the entries of the diagonal eigenvalue matrix $\omega \in \mathbb{R}^{d \times d}$. From the geometrical average of the frequencies $\bar{\omega} = (\omega_1 \cdots \omega_d)^{1/d}$ one can define the length of the harmonic oscillator $\bar{a} = \sqrt{\hbar/m\bar{\omega}}$ as a primary length scale.

2.2.1. Position representation of the Thomas–Fermi field. To cope with the physical anisotropy of the potential in the Cartesian lab-frame $\mathbf{r} = (x_1, \dots, x_d)$, it is useful to introduce a rotated, scaled frame with new coordinates defined $\mathbf{r}' = (x'_1, \dots, x'_d)$ by

$$\mathbf{r} \equiv R S \mathbf{r}', \quad (8)$$

introducing the scaling transformation $S = \sqrt{2\mu/m\omega^2}$. For each direction, the scale factors are determined by the Thomas–Fermi radii $r_{\text{TF},i} \equiv \sqrt{2\mu/m\omega_i^2}$. It is also relevant to

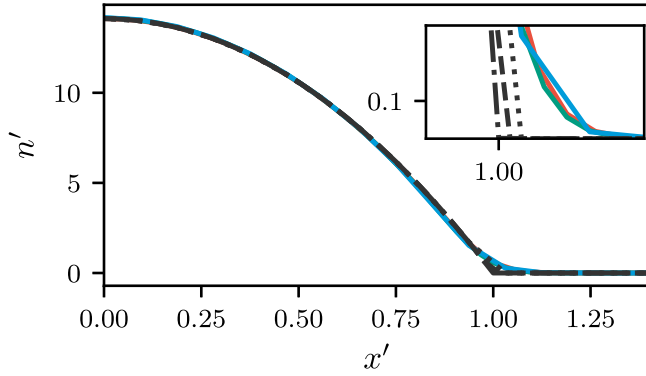


Figure 1. Ground-state position density versus Cartesian coordinate x' in a d -dimensional harmonic potential in dimensionless units: Gross–Pitaevskii solution with $d = 1$, $n'(x')$ (red —), $d = 2$, $n'(x', 0)$ (green —), $d = 3$, $n'(x', 0, 0)$ (blue —) and Thomas–Fermi density with $d = 1$, $n'_{\text{TF}}(x')$ (---), $d = 2$, $n'_{\text{TF}}(x', 0)$ (-.-.), $d = 3$, $n'_{\text{TF}}(x', 0, 0)$ (.....). We have chosen different coupling constants $\kappa = 100$ ($d = 1$), $\kappa = 625.96$ ($d = 2$) and $\kappa = 3\,547.62$ ($d = 3$) in each dimension to obtain the same chemical potential $\mu_{\text{TF}} = 14.12 \hbar\omega$. The inset shows a close-up view of the Thomas–Fermi region.

introduce the averaged radial condensate extent $r_{\text{TF}} \equiv \sqrt{2\mu/m\omega^2}$ as a secondary global length scale.

The particle normalization of the fields links the dimensional lab-coordinates amplitude $\psi(\mathbf{r})$ to the dimensionless amplitude $\psi'(r')$ in the scaled coordinates by

$$\psi'(r') \equiv r_{\text{TF}}^{\frac{d}{2}} \psi(\mathbf{r}). \quad (9)$$

In d -dimensional spherical coordinates [58], the hyper-radius $r' = \sqrt{\mathbf{r}'^2}$ is given by the Euclidean norm. The differential solid angle $d^{d-1}\Omega$, is obtained from the Cartesian volume element $d^d x' = r'^{d-1} dr' d^{d-1}\Omega$ and encompasses a total solid angle of $\Omega_d = 2\pi^{\frac{d}{2}}/\Gamma(\frac{d}{2})$. With these definitions, one finds a compact expression for the non-vanishing field

$$\psi'_{\text{TF}}(r') = \varepsilon \sqrt{1 - r'^2}, \quad \varepsilon = \sqrt{\frac{\mu}{g} \frac{r_{\text{TF}}^d}{g}}, \quad (10)$$

within the Thomas–Fermi volume (5). Here, the parameter ε denotes the ratio between chemical potential and internal energy.

An ensemble with fixed particle number N defines the chemical potential $\mu(N)$ implicitly by

$$N = \int_{V_{\text{TF}}} d^d r n_{\text{TF}}(\mathbf{r}) = \varepsilon^2 \Omega_d \int_0^1 dr' r'^{d-1} (1 - r'^2). \quad (11)$$

Evaluating the hyperradial integral, one obtain for the chemical potential [44, 46] explicitly

$$\mu(N) = \hbar\omega \left[\kappa \frac{d(d+2)}{4(2\pi)^{\frac{d}{2}}} \Gamma\left(\frac{d}{2}\right) \right]^{\frac{2}{d+2}}, \quad \kappa = \frac{gN}{\bar{a}^d \hbar\omega}. \quad (12)$$

Thus, the chemical potential exhibits a characteristic algebraic dependence on the geometric dimension, the potential shape and the internal energy κ is given in energy units of the harmonic oscillator $\hbar\omega$.

In figure 1, we depict the density of the Gross–Pitaevskii state n' , as well as the Thomas–Fermi density n'_{TF} at equal chemical potential $\mu = 14.12 \hbar\omega$. This implies different coupling constants κ for each dimension d according to (12). The inset magnifies the region around r_{TF} , where the approximation exhibits the characteristic first order discontinuity.

2.2.2. Fourier transform of the Thomas–Fermi field. In order to calculate the k space distribution of the Thomas–Fermi field (10), one has to evaluate the Fourier transform

$$\tilde{\psi}(\mathbf{k}) = \int_{-\infty}^{\infty} d^d r \frac{e^{-i\mathbf{k}\cdot\mathbf{r}}}{(2\pi)^{\frac{d}{2}}} \psi(\mathbf{r}). \quad (13)$$

According to (9), one can define a dimensionless Fourier amplitude and density

$$\tilde{\psi}(\mathbf{k}) = r_{\text{TF}}^{\frac{d}{2}} \tilde{\psi}'(\mathbf{k}'), \quad (14)$$

$$\tilde{n}'(\mathbf{k}') = |\tilde{\psi}'(\mathbf{k}')|^2, \quad (15)$$

with scaled Cartesian wave vectors

$$\mathbf{k}' = S R^{\top} \mathbf{k}. \quad (16)$$

All things considered, the dimensionless Fourier transform to the Thomas–Fermi field reads

$$\tilde{\psi}'_{\text{TF}}(\mathbf{k}') = \varepsilon \int_{V_{\text{TF}}} d^d r' \frac{e^{-i\mathbf{k}'\cdot\mathbf{r}'}}{(2\pi)^{\frac{d}{2}}} \sqrt{1 - r'^2}. \quad (17)$$

In hyper-spherical coordinates, the integral over the hyper-angles factorizes and evaluates to

$$o_d(k'r') \equiv \int_{S_{\text{TF}}} d^{d-1}\Omega \frac{e^{-i\mathbf{k}'\cdot\mathbf{r}'}}{(2\pi)^{\frac{d}{2}}} = \frac{J_{\frac{d}{2}-1}(k'r')}{(k'r')^{\frac{d}{2}-1}}, \quad (18)$$

with J_d being the Bessel function of the first kind of order d [59]. The remaining radial integral also admits a closed-form solution

$$\begin{aligned} \tilde{\psi}'_{\text{TF}}(\mathbf{k}') &= \varepsilon \int_0^1 dr' r'^{d-1} \sqrt{1 - r'^2} o_d(k'r') \\ &= \varepsilon \sqrt{\frac{\pi}{2}} o_{d+3}(k'). \end{aligned} \quad (19)$$

It is interesting to present this result with the original physical Cartesian wave-vectors

$$\tilde{\psi}(\mathbf{k}) = r_{\text{TF}}^{\frac{d}{2}} \varepsilon \sqrt{\frac{\pi}{2}} o_{d+3}\left(\sqrt{\mathbf{k}^{\top} \frac{2\mu}{m\Omega^2} \mathbf{k}}\right), \quad (20)$$

which demonstrates that the diagonalization (7) is not required to obtain the Fourier amplitude of the Thomas–Fermi field in the anisotropic oscillator in d dimensions. In particular, for the most relevant three-dimensional case, our result agrees with [36]. In figure 2, we show the momentum spectra of the numerical Gross–Pitaevskii field and the analytical Thomas–Fermi solution (19). As a guide to the eye, we have added algebraic k'^{d-2} and exponential $e^{-k'/2}$ envelopes to match the asymptotic behavior.

To foster physical interpretation and to choose suitable numerical grids in simulations of the Gross–Pitaevskii equation, it is important to understand the high energy

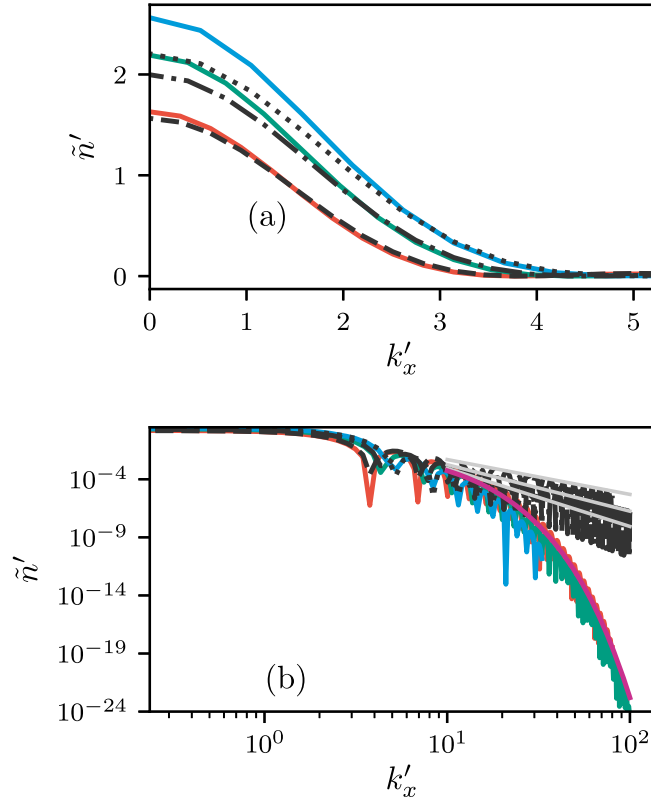


Figure 2. (a) Ground-state Fourier density versus scaled Cartesian wave-number k'_x in a d -dimensional harmonic potential in dimensionless units: Gross-Pitaevskii density for $d = 1$, $\tilde{n}'(k'_x)$ (red —), $d = 2$, $\tilde{n}'(k'_x, 0)$ (green —), $d = 3$, $\tilde{n}'(k'_x, 0, 0)$ (blue —) and Thomas-Fermi density for $d = 1$, $\tilde{n}'_{\text{TF}}(k'_x)$ (---), $d = 2$, $\tilde{n}'_{\text{TF}}(k'_x, 0)$ (-·-·), $d = 3$, $\tilde{n}'_{\text{TF}}(k'_x, 0, 0)$ (·····). (b) The double logarithmic plot shows the high energy algebraic decay $\sim k'^{-d-2}$ (gray —) of $\tilde{n}'_{\text{TF}}(k')$, and an exponential $\sim e^{-k'/2}$ decay (magenta —) for the numerical Gross-Pitaevskii density. All parameters are chosen as in figure 1.

behavior of the Fourier amplitude. From the asymptotic representation of the Bessel functions, one finds a periodic oscillation with algebraic decay

$$\tilde{\psi}'_{\text{TF}}(\mathbf{k}' \rightarrow \infty) \sim \varepsilon \frac{\sin\left(k' - \frac{d\pi}{4}\right)}{k'^{\frac{d+2}{2}}}. \quad (21)$$

For small wave vectors, the Fourier amplitude stays regular and approaches

$$\tilde{\psi}'_{\text{TF}}(\mathbf{k}' \rightarrow 0) \sim \frac{\varepsilon}{2^{\frac{d+2}{2}} \Gamma\left(\frac{d+3}{2}\right)}. \quad (22)$$

The Heisenberg uncertainty principle of quantum-physics and the uncertainty relation of harmonic analysis [60]

$$\Delta r \Delta k \geq \frac{d}{2}, \quad (23)$$

are connected by the de Broglie relation $p = \hbar k$ [1]. It provides the basis for the rule-of-thumb estimate of a minimal width, i.e., the standard deviation of the Thomas-Fermi field

Table 1. Widths in k space according to the Rayleigh and Heisenberg criterion for a Thomas-Fermi radius of $r_{\text{TF}} = 10 \mu\text{m}$.

	Solid angle	Bessel zero	Rayleigh width	Heisenberg width	%
d	Ω_d	k'_1	$\Delta k_{\text{TF}}^{\text{R}}$	$\Delta k_{\text{TF}}^{\text{H}}$	β
1	2	3.83	$0.38 \mu\text{m}^{-1}$	$0.05 \mu\text{m}^{-1}$	0.98
2	2π	4.49	$0.45 \mu\text{m}^{-1}$	$0.10 \mu\text{m}^{-1}$	0.95
3	4π	5.14	$0.51 \mu\text{m}^{-1}$	$0.15 \mu\text{m}^{-1}$	0.93

in k space

$$\Delta k_{\text{TF}}^{\text{H}} \geq \frac{d}{2r_{\text{TF}}}, \quad (24)$$

if the Thomas-Fermi radius is a measure of the position width $\Delta r = r_{\text{TF}}$.

Alternatively, we can specify a width of the Thomas-Fermi field (19) according to the Rayleigh criterion

$$\Delta k_{\text{TF}}^{\text{R}} = \frac{k'_1}{r_{\text{TF}}}, \quad (25)$$

by the first root of the Bessel function $J_{\frac{d+1}{2}}(k'_1) = 0$. Then, the fraction of atoms

$$\beta \equiv N^{-1} \int_{-\infty}^{\infty} d^d q' \theta(k'_1 - q') |\tilde{\psi}_{\text{TF}}(\mathbf{q}')|^2, \quad (26)$$

measures the localization of the spectrum for wave numbers $q' \leq k'_1$. In table 1 we have summarized these parameters as a function of dimension.

3. Thomas-Fermi Wigner function

The spatial extent r_{TF} and width Δk_{TF} of the Thomas-Fermi field are very important quantities and can be found from the position, or Fourier distribution, as discussed in the previous section. However, complete information on the field is only encompassed by the Wigner function in phase space [22, 26]

$$W(\mathbf{r}, \mathbf{k}) = \int_{-\infty}^{\infty} d^d \xi \frac{e^{-i\mathbf{k}\cdot\xi}}{(2\pi)^d} \rho(\mathbf{r}, \xi), \quad (27)$$

which is defined by the Fourier transform of the coherence function

$$\rho(\mathbf{r}, \xi) = \psi\left(\mathbf{r} + \frac{\xi}{2}\right) \psi^*\left(\mathbf{r} - \frac{\xi}{2}\right). \quad (28)$$

Position and Fourier densities are the marginal distributions of the Wigner function

$$|\tilde{\psi}(\mathbf{k})|^2 = \int_{-\infty}^{\infty} d^d r W(\mathbf{r}, \mathbf{k}), \quad (29)$$

$$|\psi(\mathbf{r})|^2 = \int_{-\infty}^{\infty} d^d k W(\mathbf{r}, \mathbf{k}). \quad (30)$$

The Wigner function is only a quasi-probability distribution, as it can acquire negative values. This is not a bug but the central feature of interference of waves in phase-space [61].

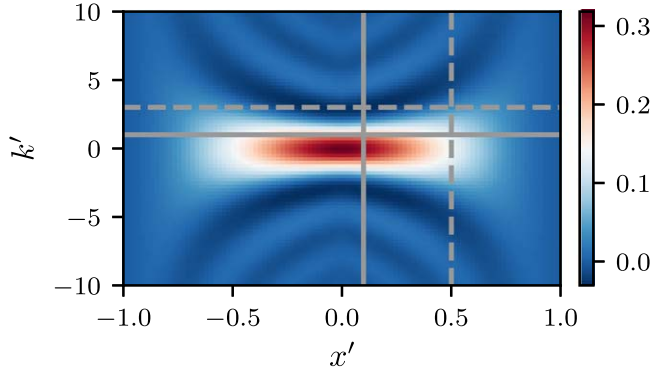


Figure 3. Color-coded density plot of the numerically calculated Thomas–Fermi Wigner function $W'_{\text{TF}}(x', k')$ for a one-dimensional harmonic oscillator in phase-space. Cross-sections along the phase-space coordinates $x' = \{0.1, 0.5\}$ and $k' = \{1.0, 3.0\}$ are marked by the gray lines (—, - - -) and are depicted in figures 5 and 6. The parameters are $\kappa = 100$ and $\mu_{\text{TF}} = 14.12 \hbar\omega$.

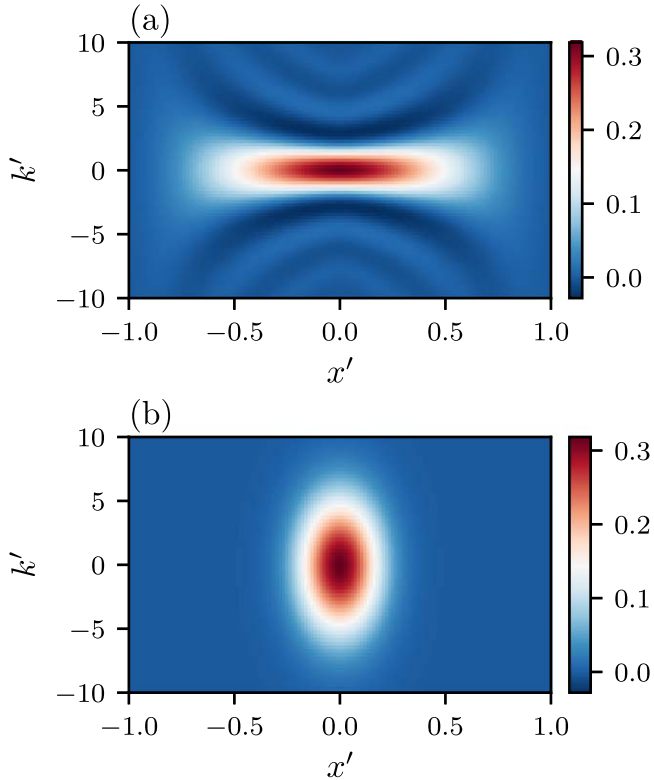


Figure 4. Color-coded density plot of the Gross–Pitaevskii Wigner function $W'(x', k')$ for the ground state in an one-dimensional harmonic potential. In subfigure (a), we have strong interaction $\kappa = 100$, $\mu = 14.11 \hbar\omega$ and weak interaction $\kappa = 0.1$, $\mu = 0.54 \hbar\omega$ in subfigure (b).

3.1. Thomas–Fermi Wigner function in a one-dimensional harmonic oscillator

For the one-dimensional harmonic oscillator potential

$$v(x) = \frac{1}{2}m\omega^2x^2, \quad (31)$$

the Thomas–Fermi coherence function (10), (28) evaluates to

$$\rho'_{\text{TF}}(x', \xi') = \varepsilon^2 \left[(1 - x'^2)^2 - (1 + x'^2) \frac{\xi'^2}{2} + \frac{\xi'^4}{16} \right]^{\frac{1}{2}}, \quad (32)$$

when $|x'| < 1$ and $|\xi'| < \xi'_+(x') \equiv 2(1 - |x'|)$. It vanishes otherwise. This leads to

$$W'_{\text{TF}}(x', k') = \int_{-\xi'_+(x')}^{\xi'_+(x')} d\xi' \frac{e^{-ik'\xi'}}{2\pi} \rho'_{\text{TF}}(x', \xi'). \quad (33)$$

Now, this Wigner function depends on dimensionless phase-space coordinates $(x', k') = (x/x_{\text{TF}}, k/x_{\text{TF}})$, and $x_{\text{TF}} = \sqrt{2\mu/m\omega^2}$ denotes the Thomas–Fermi size of the one-dimensional harmonic oscillator.

The Fourier-integral (33) can be evaluated easily by numerical quadrature and is shown in figure 3. In the Thomas–Fermi regime $\mu \gg \hbar\omega$, the mean-field pressure increases the spatial size beyond the harmonic oscillator size $r_{\text{TF}} \gg \bar{a}$, but squeezes in the k -direction reciprocally. The negative domains of the Wigner function can be seen clearly by dark blue stripes.

We have already compared the numerical exact Gross–Pitaevskii field with the Thomas–Fermi approximation in position space in figure 1 and reciprocal space in figure 2. In figure 4, we depict the full phase-space representation of the numerical Gross–Pitaevskii field (3) with strong interactions in subfigure (a). Indeed, the two-dimensional phase-space density plot exhibits the same qualitative appearance as in figure 3. However, the more detailed cross-section plots of figures 5 and 6 highlights the deviations. In subfigure (b), we recover the positive Gaussian phase-space distribution of a coherent state for weak interaction.

3.2. Factorizing the coherence function

Despite the functional simplicity of the Thomas–Fermi Wigner function, we have not succeeded in finding a closed form expression. Therefore, we consider the physical factorization ansatz for the coherence function (33)

$$\rho'_{\text{TF}}(x', \xi') = n'_{\text{TF}}(x') \chi\left(\frac{\xi'}{\eta(x')}\right), \quad (34)$$

$$n'_{\text{TF}}(x') = \varepsilon^2(1 - x'^2), \quad (35)$$

$$\chi(\xi') = 1 - \frac{\xi'^2}{4}, \quad (36)$$

including an unspecified x -dependent scale $\eta(x)$. With a suitable scale, the factorized coherence function $\rho'_{\text{TF}}(x', \xi')$ has the same support in phase-space as the full coherence function (32). By choosing the scale $\eta(x') = \xi'_+(x')/2$, one obtains the Wigner function as

$$W'_{\text{TF}}(x', k') = n'_{\text{TF}}(x') \frac{2j_1[k'\xi'_+(x')]}{\pi k'}, \quad (37)$$

where j_1 is the spherical Bessel function of order one. Equation (37) matches the numerical simulations quite well for various values of x and k as regarded in figures 5 and 6.

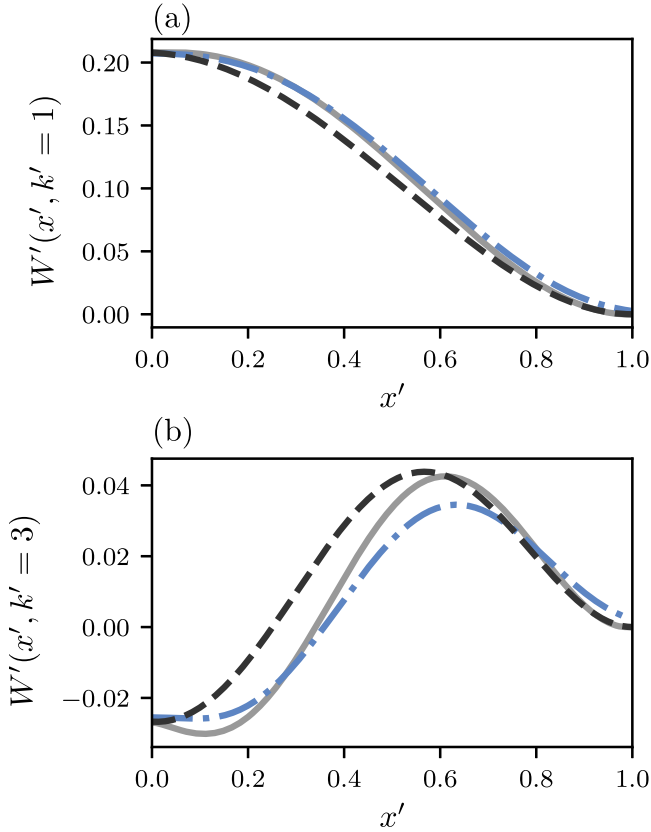


Figure 5. Cross-section of the Wigner function versus x' for fixed wave-number k' for the one-dimensional harmonic oscillator. Comparison of Thomas–Fermi approximation $W'_{\text{TF}}(x', k')$ (gray —), with the Gross–Pitaevskii Wigner function $W'(x', k')$ (blue - - -) and the factorizing approach $W'_{\text{TF}}(x', k')$ (37) (black - - -). We have chosen the same parameters as in figure 3: (a) $k' = 1.0$, (b) $k' = 3.0$.

Further, the factorized Wigner function (37) features the correct marginal distribution (30)

$$n'_{\text{TF}}(x') = n'_{\text{TF}}(x') \geq 0, \quad (38)$$

$$\tilde{n}'_{\text{TF}}(k') = \frac{\varepsilon^2}{\pi k'^4} [2k' \text{Si}(2k') + \cos 2k' - k' \sin 2k' - 1] \geq 0, \quad (39)$$

where Si denotes the sine-integral [59].

The Fourier density $\tilde{n}'_{\text{TF}}(k')$ is shown in figure 7. In contrast to the analytical result (19), it lacks the nodal structure and shows small k deviations. Nevertheless, it is positive and exhibits the same algebraic asymptotics $\tilde{n}'_{\text{TF}}(k' \rightarrow \infty) \sim \varepsilon^2 k'^{-3}$, as (21).

3.3. Thomas–Fermi Wigner function of an anisotropic oscillator

In section 2.2.1, we have considered an anisotropic tilted harmonic oscillator and defined the coordinate transformation (8) between lab- and body-fixed scaled coordinates. In turn, this induces a relation between the field amplitudes in the two frames (9). For the Wigner representation this transformation reads

$$W'(\mathbf{r}', \mathbf{k}') \equiv W(\mathbf{r}, \mathbf{k}). \quad (40)$$

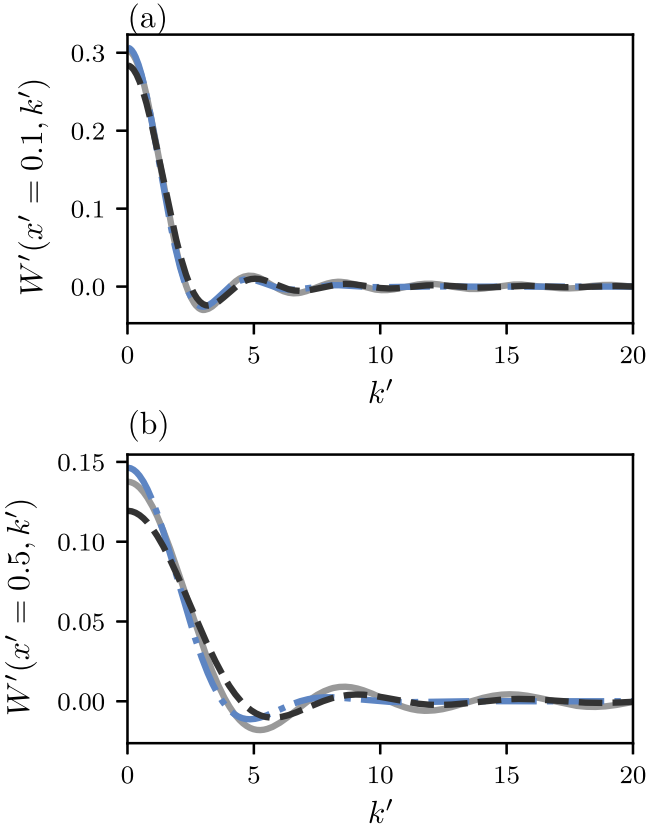


Figure 6. Cross-section of the Wigner function versus k' for fixed position x' for the one-dimensional harmonic oscillator. Comparison of Thomas–Fermi approximation $W'_{\text{TF}}(x', k')$ (gray —), with the Gross–Pitaevskii Wigner function $W'(x', k')$ (blue - - -) and the factorizing approach $W'_{\text{TF}}(x', k')$ (37) (black - - -). We have chosen the same parameters as in figure 3: (a) $x' = 0.1$, (b) $x' = 0.5$.

In the body-fixed scaled coordinates, the Thomas–Fermi field (10) is an isotropic s -wave. Thus, the Wigner function $W'_{\text{TF}}(\mathbf{r}', \mathbf{k}') = W'_{\text{TF}}(r', k', \mathbf{r}' \cdot \mathbf{k}')$ must depend only on the three rotation invariant scalars [62], denoting the enclosed angle as $\theta_k = \angle(\mathbf{r}', \mathbf{k}')$. This rotation invariance can be also seen directly in the coherence function

$$W'_{\text{TF}}(\mathbf{r}', \mathbf{k}') = \int_{-\infty}^{\infty} d^3 \xi' \frac{e^{-i\mathbf{k}' \cdot \xi'}}{(2\pi)^3} \rho'_{\text{TF}}(\mathbf{r}', \xi'), \quad (41)$$

$$\rho'_{\text{TF}}(\mathbf{r}', \xi') = \varepsilon^2 \sqrt{\left(1 - r'^2 - \frac{\xi'^2}{4}\right)^2 - (\mathbf{r}' \cdot \xi')^2}. \quad (42)$$

In figure 8, we have depicted a two-dimensional cross-section (x', k'_x) of the six-dimensional Thomas–Fermi Wigner function using numerical quadrature.

3.3.1. Spherical coordinates. If the integration variable ξ' is expressed in spherical coordinates (ξ', θ, ϕ) with \mathbf{r}' aligned with the z' -direction and $\mathbf{k}' \in x'-z'$ plane, then $\theta = \angle(\mathbf{r}', \xi')$ denotes the polar angle. The coherence function $\rho'_{\text{TF}}(r', \xi', \theta)$

$$\rho'_{\text{TF}} = \varepsilon^2 \left[\left(1 - r'^2 - \frac{\xi'^2}{4}\right)^2 - (r' \xi' \cos \theta)^2 \right]^{\frac{1}{2}}, \quad (43)$$

$$\xi'(r', \theta) \equiv 2 \sqrt{1 - r'^2 \sin^2 \theta - r' |\cos \theta|} \quad (44)$$

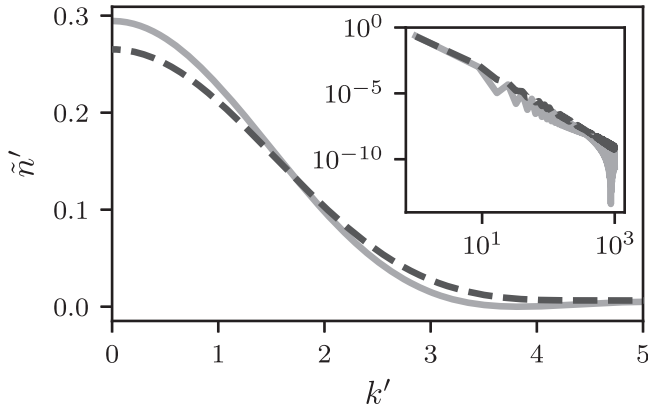


Figure 7. Fourier density $\tilde{n}'_{\text{TF}}(k')$ of the Thomas–Fermi approximation versus wave-number k' in a one-dimensional oscillator (19) (— line) and $\tilde{n}'_{\text{TF}}(k')$ of the factorized Wigner function (39) (- - line). The double logarithmic inset displays the algebraic decay for large k' .

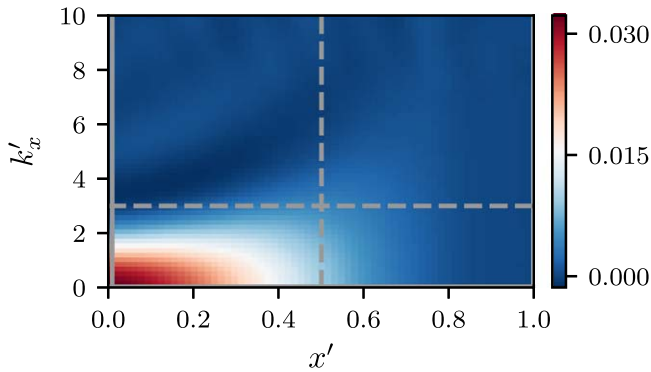


Figure 8. Color-coded two-dimensional cross-section of the six-dimensional Cartesian Thomas–Fermi Wigner function $W'_{\text{TF}}(x', 0, 0, k'_x, 0, 0)$ for the isotropic three-dimensional harmonic oscillator in phase space. Cross-sections along the phase-space coordinates $x' = \{0.0, 0.5\}$ and $k'_x = \{0.0, 3.0\}$ are marked by the gray lines (—, - - -) and are depicted in figures 10 and 11. The parameters are $\kappa = 100$ and $\mu_{\text{TF}} = 3.38 \hbar\omega$.

is finite only, when $r' < 1$ and $\xi' < \xi'(r', \theta)$. Exploiting the axial-symmetry of the coherence function yields the Wigner function as

$$W'_{\text{TF}}(r', k', \theta_k) = \int_0^\pi d\theta \sin \theta \int_0^{\xi'(r', \theta)} d\xi' \xi'^2 \times J_0(k'_x \xi'_x) \frac{e^{-ik'_z \xi'_z}}{(2\pi)^2} \rho'_{\text{TF}}(r', \xi', \theta), \quad (45)$$

where $k'_x = k' \sin \theta_k$, $k'_z = k' \cos \theta_k$ and $\xi'_x = \xi' \sin \theta$, $\xi'_z = \xi' \cos \theta$. Unfortunately, no further simplification of the two-dimensional integral was found.

3.3.2. Cylinder coordinates. If the integration variable ξ' is expressed in cylindrical coordinates (ξ', ϕ, ζ) , aligning the cylinder axis on r' and $k' \in x'$ - z' plane, then the coherence

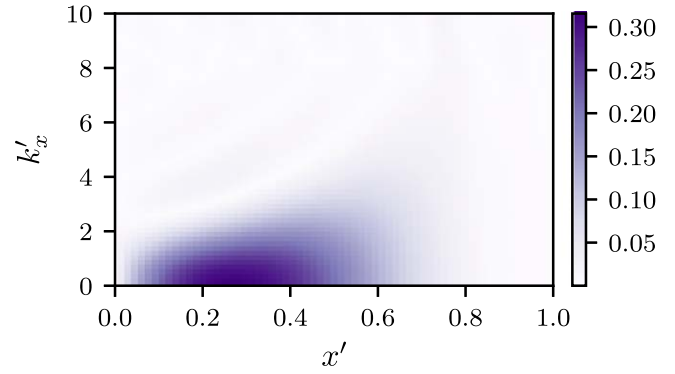


Figure 9. Color-coded two-dimensional cross-section of the relative deviation $\Delta(x', 0, 0, k'_x, 0, 0)$ of the exact evaluation and the analytical approximation of the Thomas–Fermi Wigner function (54) for the isotropic three-dimensional harmonic oscillator.

function $\rho'_{\text{TF}}(r', \xi', \zeta')$

$$\rho'_{\text{TF}} = \varepsilon^2 \left[\left(1 - r'^2 - \frac{\xi'^2 + \zeta'^2}{4} \right)^2 - (r' \zeta')^2 \right]^{\frac{1}{2}}, \quad (46)$$

$$\zeta'(r', \xi') \equiv \sqrt{4 - \xi'^2} - 2r' \geq 0, \quad (47)$$

$$\xi'(r') \equiv 2\sqrt{1 - r'^2}, \quad (48)$$

is non-vanishing only, when $|r'| < 1$, $|\zeta'| < \xi'(r')$, and $|\zeta'| < \zeta'(r', \xi')$. Then, the Wigner function reads

$$W'_{\text{TF}}(r', k', \theta_k) = \int_0^{\xi'(r')} d\xi' \xi' J_0(k'_x \xi') \int_{-\zeta'(r', \xi')}^{\zeta'(r', \xi')} d\zeta' \times \frac{e^{-ik'_z \zeta'}}{(2\pi)^2} \rho'_{\text{TF}}(r', \xi', \zeta'), \quad (49)$$

with $k'_x = k' \sin \theta_k$ and $k'_z = k' \cos \theta_k$. No further simplification was found.

3.4. Factorizing the three-dimensional coherence function

The analytical evaluation of the Fourier-transformation of the coherence function did not lead to simple closed form expressions for the Wigner function. Therefore, we have resorted to the factorization ansatz of the coherence function

$$\rho'_{\text{TF}}(\mathbf{r}', \boldsymbol{\xi}') = n'_{\text{TF}}(r') \chi\left(\frac{\xi'}{\eta(r', \theta)}\right), \quad (50)$$

$$n'_{\text{TF}}(r') = \varepsilon^2 (1 - r'^2), \quad (51)$$

$$\chi(\xi') = 1 - \frac{\xi'^2}{4}. \quad (52)$$

As in the one-dimensional case, one can choose a scale $\eta(r', \theta) = \xi'(r', \theta)/2$ such that the support of the factorized coherence function (50) matches the full coherence function (43) and (44).

In general, the shape of the support of the coherence function changes continuously with r' from a sphere to a lenticular form of decreasing volume. If one considers only the inscribed sphere with radius $\xi'(r') = 2(1 - r')$, then the scale also simplifies to $\eta(r') = 1 - r'$, being independent of θ . All

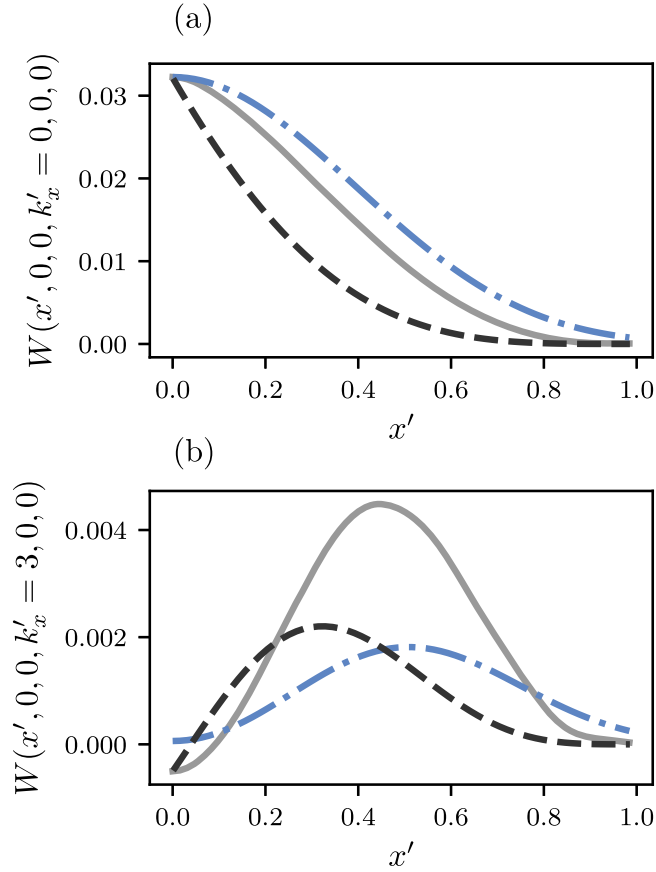


Figure 10. Cross-section of the Wigner function versus x' for fixed wave-number k'_x for the isotropic three-dimensional harmonic oscillator. Comparison of Thomas–Fermi approximation $W'_{\text{TF}}(x', 0, 0, k'_x, 0, 0)$ (gray —), with the Gross–Pitaevskii Wigner function $W'(x', 0, 0, k'_x, 0, 0)$ (blue - · -) and the factorizing approach $W'_{\text{TF}}(x', 0, 0, k'_x, 0, 0)$ (53) (black - - -). We have chosen the same parameters as in figure 8: (a) $k'_x = 0.0$, (b) $k'_x = 3.0$.

things considered, this leads to the isotropic contribution of the Wigner function with the factorization assumption

$$W'_{\text{TF}}(r', k') = n'_{\text{TF}}(r') \xi'(r') \frac{j_2[k' \xi(r')]}{\pi^2 k'^2}. \quad (53)$$

In figure 9, we plot the relative deviation

$$\Delta(r', k') = \frac{\pi^3}{N} |W'_{\text{TF}}(r', k') - W'_{\text{TF}}(r', k')|, \quad (54)$$

of the numerical and the factorized Thomas–Fermi Wigner function with respect to the maximal attainable value [26]. Significant deviations are noticeable at the flanks of the distribution. This behavior can be studied in greater detail analyzing cross-sections of the Wigner function at a fixed wave-number in figure 10 and fixed position in figure 11.

The marginal distributions of (53) read

$$n'_{\text{TF}}(r') = n'_{\text{TF}}(r') \geq 0, \quad (55)$$

$$n'_{\text{TF}}(k') = \frac{\varepsilon^2}{\pi k'^6} [6k' \text{Si}(2k') + 2(k'^2 + 2) \cos(2k') - 3k' \sin(2k') - 4] \leq 0, \quad (56)$$

where one recovers the correct positive Thomas–Fermi

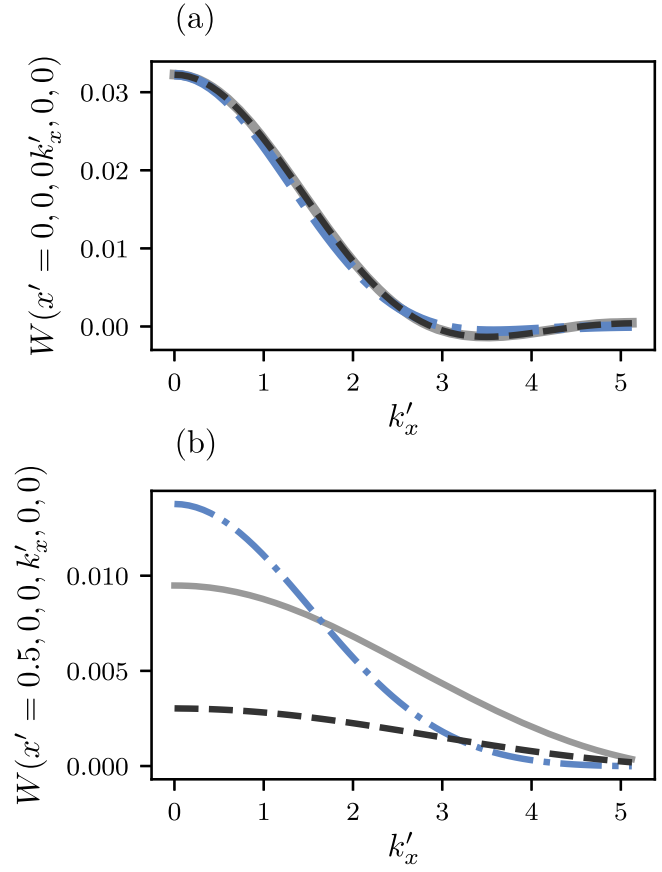


Figure 11. Cross-section of the Wigner function versus k'_x for fixed position x' for the isotropic three-dimensional harmonic oscillator. Comparison of Thomas–Fermi approximation $W'_{\text{TF}}(x', 0, 0, k'_x, 0, 0)$ (gray —), with the Gross–Pitaevskii Wigner function $W'(x', 0, 0, k'_x, 0, 0)$ (blue - · -) and the factorizing approach $W'_{\text{TF}}(x', 0, 0, k'_x, 0, 0)$ (53) (black - - -). We have chosen the same parameters as in figure 8: (a) $x' = 0$, (b) $x' = 0.5$.

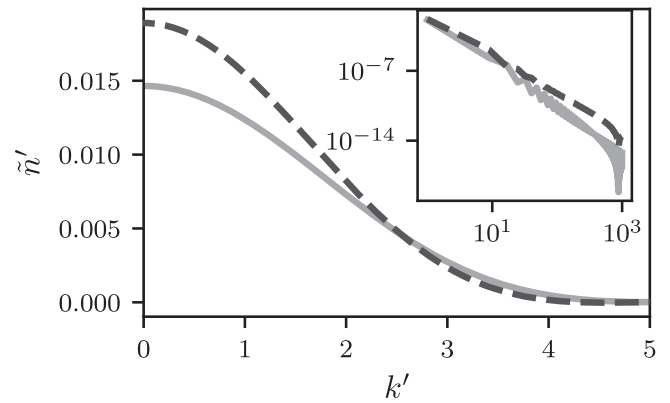


Figure 12. Fourier density $\tilde{n}'_{\text{TF}}(k')$ of the Thomas–Fermi approximation (19) versus wave-number k' in an isotropic three-dimensional harmonic oscillator (— line) and $\tilde{n}'_{\text{TF}}(k')$ of the factorized Wigner function (56) (- - line). The double logarithmic inset displays the algebraic decay for large k' .

density. Due to approximate scaling factor, some integration volume is lost and one misses some contributions to the Fourier density such that the strict positivity is marginally violated. This is depicted in figure 12.

4. Conclusion and outlook

The Wigner phase-space description is a central concept in classical optics, signal processing and matter-wave optics. In the case of interaction dominated Bose-condensed gases, one can use the Thomas–Fermi approximation of the Gross–Pitaevskii equation. For physical interpretations and applications in ray tracing simulations, it is of relevance to have reliable and simple parametrizations of the Thomas–Fermi Wigner phase-space distribution. We present some simple approximations within the additional factorization approach and analyze their deviations. However, a systematic expansion procedure in the spirit of a multi-pole expansion, or more generally for partially coherent fields as in the Gaussian Schell model of classical beam-optics [63] is still lacking.

Acknowledgments

We gratefully acknowledge support from the German Aeronautics and Space Administration (DLR) through Grant no. 50 WM 1557.

References

- [1] De Broglie L 1925 Recherches sur la théorie des quanta *Ann. Phys.* **10** 22–128
- [2] Davisson C and Germer L H 1927 Diffraction of electrons by a crystal of nickel *Phys. Rev.* **30** 705–40
- [3] Adams C S, Sigel M and Mlynek J 1994 Atom optics *Phys. Rep.* **240** 143–210
- [4] Berman P R 1997 *Atom Interferometry* (New York: Academic)
- [5] Peters A, Chung K Y and Chu S 1999 Measurement of gravitational acceleration by dropping atoms *Nature* **400** 849–52
- [6] Peters A, Chung K Y and Chu S 2001 High-precision gravity measurements using atom interferometry *Metrologia* **38** 25
- [7] Nandi G, Walser R, Kajari E and Schleich W P 2007 Dropping cold quantum gases on earth over long times and large distances *Phys. Rev. A* **76** 63617
- [8] Stockton J K, Takase K and Kasevich M A 2011 Absolute geodetic rotation measurement using atom interferometry *Phys. Rev. Lett.* **107** 133001
- [9] Hu Z-K, Sun B-L, Duan X-C, Zhou M-K, Chen L-L, Zhan S, Zhang Q-Z and Luo J 2013 Demonstration of an ultrahigh-sensitivity atom-interferometry absolute gravimeter *Phys. Rev. A* **88** 043610
- [10] Aguilera D N et al 2014 STE-QUEST-test of the universality of free fall using cold atom interferometry *Class. Quantum Grav.* **31** 115010
- [11] Becker D et al 2018 Space-borne Bose–Einstein condensation for precision interferometry *Nature* accepted (<https://doi.org/10.1038/s41586-018-0605-1>)
- [12] Einstein A 1924 Quantentheorie des einatomigen idealen Gases *Sitzungsber. Preuss. Akad. Wiss.* **22** 261
- [13] Einstein A 1925 Quantentheorie des einatomigen idealen Gases: Zweite Abhandlung *Sitzungsber. Preuss. Akad. Wiss.* **1** 3
- [14] Anderson M H, Ensher J R, Matthews M R, Wieman C E and Cornell E A 1995 Observation of Bose–Einstein condensation in a dilute atomic vapor *Science* **269** 198–201
- [15] Davis K B, Mewes M-O, Andrews M R, Van Druten N J, Durfee D S, Kurn D M and Ketterle W 1995 Bose–Einstein condensation in a gas of sodium atoms *Phys. Rev. Lett.* **75** 3969
- [16] Bradley C I C, Sackett C A, Tollett J J and Hulet R G 1995 Evidence of Bose–Einstein condensation in an atomic gas with attractive interactions *Phys. Rev. Lett.* **75** 1687
- [17] Kozuma M, Deng L, Hagley E W, Wen J, Lutwak R, Helmerson K, Rolston S L and Phillips W D 1999 Coherent splitting of Bose–Einstein condensed atoms with optically induced Bragg diffraction *Phys. Rev. Lett.* **82** 871–5
- [18] Bongs K, Burger S, Birkel G, Sengstock K, Ertmer K, Rządowski K, Sanpera A and Lewenstein M 1999 Coherent evolution of bouncing Bose–Einstein condensates *Phys. Rev. Lett.* **83** 3577–80
- [19] Dumke R, Mütter T, Volk M, Ertmer W and Birkel G 2002 Interferometer-type structures for guided atoms *Phys. Rev. Lett.* **89** 220402
- [20] Cassettari D, Hessmo B, Folman R, Maier T and Schmiedmayer J 2000 Beam splitter for guided atoms *Phys. Rev. Lett.* **85** 5483–7
- [21] Kovachy T, Hogan J M, Sugarbaker A, Dickerson S M, Donnelly C A, Overstreet C and Kasevich M A 2015 Matter wave lensing to picokelvin temperatures *Phys. Rev. Lett.* **114** 143004
- [22] Wigner E 1932 On the quantum correction for thermodynamic equilibrium *Phys. Rev.* **40** 749–59
- [23] Kadanoff L P and Baym G 1962 *Quantum Statistical Mechanics* (New York: W A Benjamin)
- [24] Cahill K E and Glauber R J 1969 Density operators and quasiprobability distributions *Phys. Rev.* **177** 1882–902
- [25] Balescu R 1975 *Equilibrium and Nonequilibrium Statistical Mechanics* (New York: Wiley)
- [26] Schleich W P 2015 *Quantum Optics in Phase Space* (New York: Wiley)
- [27] Steel M J, Olsen M K, Plimak L I, Drummond P D, Tan S M, Collett M J, Walls D F and Graham R 1998 Dynamical quantum noise in trapped Bose–Einstein condensates *Phys. Rev. A* **58** 4824–35
- [28] Sinatra A, Lobo C and Castin Y 2002 The truncated Wigner method for Bose-condensed gases: limits of validity and applications *J. Phys. B: At. Mol. Opt. Phys.* **35** 3599
- [29] Griffin A, Nikuni T and Zaremba E 2009 *Bose-Condensed Gases at Finite Temperature* (Cambridge: Cambridge University Press)
- [30] Walser R, Williams J, Cooper J and Holland M 1999 Quantum kinetic theory for a condensed bosonic gas *Phys. Rev. A* **59** 3878
- [31] Walser R, Cooper J and Holland M 2001 Reversible and irreversible evolution of a condensed bosonic gas *Phys. Rev. A* **63** 013607
- [32] Gross E P 1961 Structure of a quantized vortex in boson systems *Il Nuovo Cimento* **20** 454–77
- [33] Pitaevskii L P 1961 Vortex lines in an imperfect Bose gas *Sov. Phys. JETP* **13** 451–4
- [34] Thomas L H 1927 The calculation of atomic fields *Mathematical Proc. of the Cambridge Philosophical Society* **23** 542–8
- [35] Fermi E 1928 Eine statistische Methode zur Bestimmung einiger Eigenschaften des Atoms und ihre Anwendung auf die Theorie des periodischen Systems der Elemente *Zeitschrift für Physik* **48** 73–9
- [36] Baym G and Pethick C J 1996 Ground-state properties of magnetically trapped Bose-condensed Rubidium gas *Phys. Rev. Lett.* **76** 6–9
- [37] Stringari S 1996 Collective excitations of a trapped Bose-condensed gas *Phys. Rev. Lett.* **77** 2360
- [38] Castin Y and Dum R 1996 Bose–Einstein condensates in time dependent traps *Phys. Rev. Lett.* **77** 5315–9

- [39] Kagan Y, Surkov E L and Shlyapnikov G V 1996 Evolution of a Bose-condensed gas under variations of the confining potential *Phys. Rev. A* **54** R1753–6
- [40] Bordé C J 2001 Theoretical tools for atom optics and interferometry *Comptes Rendus de l'Académie des Sciences—Series IV—Physics* **2** 509–30
- [41] Impens F and Guéry-Odelin D 2010 Classical phase-space approach for coherent matter waves *Phys. Rev. A* **81** 065602
- [42] Chen J and Lin Q 2008 Partially coherent matter wave and its evolution *Opt. Commun.* **281** 1300–5
- [43] Walraven J 2018 Quantum gases Lecture notes <https://staff.fnwi.uva.nl/j.t.m.walraven/walraven/Lectures.html>
- [44] Bagnato V, Pritchard D E and Kleppner D 1987 Bose–Einstein condensation in an external potential *Phys. Rev. A* **35** 4354–8
- [45] Ruprecht P A, Holland M J, Burnett K and Edwards M 1995 Time-dependent solution of the nonlinear Schrödinger equation for Bose-condensed trapped neutral atoms *Phys. Rev. A* **51** 4704–11
- [46] Pethick C J and Smith H 2008 *Bose–Einstein Condensation in Dilute Gases* 2nd edn (Cambridge: Cambridge University Press)
- [47] Pitaevskii L P and Stringari S 2003 *Bose–Einstein Condensation (International Series of Monographs on Physics)* (Oxford: Clarendon)
- [48] Hohenberg P C 1967 Existence of long-range order in one and two dimensions *Phys. Rev.* **158** 383
- [49] Mermin N D and Wagner H 1966 Absence of ferromagnetism or antiferromagnetism in one- or two-dimensional isotropic Heisenberg models *Phys. Rev. Lett.* **17** 1133
- [50] Bagnato V and Kleppner D 1991 Bose–Einstein condensation in low-dimensional traps *Phys. Rev. A* **44** 7439–41
- [51] Fetter A L and Feder D L 1998 Beyond the Thomas–Fermi approximation for a trapped condensed Bose–Einstein gas *Phys. Rev. A* **58** 3185–94
- [52] Grimm R, Weidemüller M and Ovchinnikov Y B 2000 Optical dipole traps for neutral atoms *Advances In Atomic, Molecular, and Optical Physics* **42** (New York: Academic) pp 95–170
- [53] Bergeman T, Erez G and Metcalf H J 1987 Magnetostatic trapping fields for neutral atoms *Phys. Rev. A* **35** 1535–46
- [54] Schmiedmayer J 1995 Guiding and trapping a neutral atom on a wire *Phys. Rev. A* **52** R13–6
- [55] Fortagh J, Grossmann A, Zimmermann C and Hänsch T W 1998 Miniaturized wire trap for neutral atoms *Phys. Rev. Lett.* **81** 5310–3
- [56] Hänsel W, Hommelhoff P, Hänsch T W and Reichel J 2001 Bose–Einstein condensation on a microelectronic chip *Nature* **413** 498–501
- [57] Keil M, Amit O, Zhou S, Groswasser D, Japha Y and Folman R 2016 Fifteen years of cold matter on the atom chip: promise, realizations, and prospects *J. Mod. Opt.* **63** 1840–85
- [58] Dahl J P, Greenberger D M, Hall M J W, Sussmann G, Wolf A and Schleich W P 2005 Adventures in s-waves *Laser Phys.* **15** 18–38
- [59] Abramowitz M and Stegun I 1972 *Handbook of Mathematical Functions with Formulas, Graphs, and Mathematical tables* (New York: Dover Publications)
- [60] Folland G and Sitaram A 1997 The uncertainty principle: a mathematical survey *Journal of Fourier Analysis and Applications* **3** 207–38
- [61] Schleich W P and Wheeler J A 1987 Oscillations in photon distribution of squeezed states and interference in phase space *Nature* **326** 574
- [62] Dahl J P, Varro S, Wolf A and Schleich W P 2007 Wigner functions of s waves *Phys. Rev. A* **75** 052107
- [63] Starikov A and Wolf E 1982 Coherent-mode representation of Gaussian Schell model sources and of their radiation fields *J. Opt. Soc. Am.* **72** 923–8